Journal of Colloid and Interface Science 654 (2024) 848–858

Contents lists available at ScienceDirect

Journal of Colloid And Interface Science

journal homepage: www.elsevier.com/locate/jcis

Controlling plasmonic suprastructures through self-assembly of gold nanoparticles with hybrid copolymer-lipid vesicles

Jacopo Cardellini [a,1], Arianna Balestri [a,1], Luca Comparini [a,2], Barbara Lonetti [b], Marco Brucale [c], Francesco Valle [c], Debora Berti [a], Costanza Montis [a,*]

[a] Department of Chemistry, University of Florence, and CSGI, Florence, Italy
[b] Laboratoire des IMRCP, Université de Toulouse, CNRS, Toulouse 31062, France
[c] CNR and CSGI, Bologna, Italy

GRAPHICAL ABSTRACT

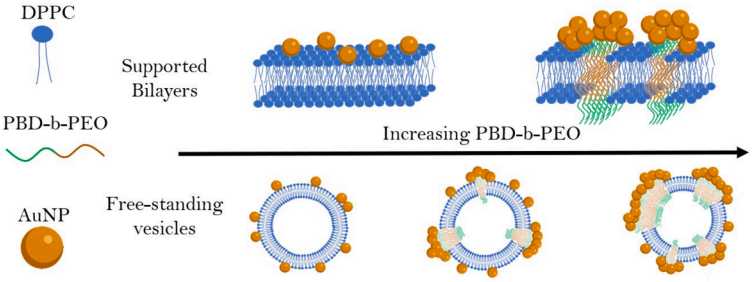

ARTICLE INFO

Keywords:
Polymersomes
Lipid vesicles
Hybrid membranes
Gold nanoparticles
Nano-bio interfaces
Plasmonic materials

ABSTRACT

Hybrid lipid membranes incorporating amphiphilic copolymers have gained significant attention due to their potential applications in various fields, including drug delivery and sensing. By combining the properties of copolymers and lipid membranes, such as enhanced chemical tunability and stability, environmental responsiveness, and multidomain nature, novel membrane architectures have been proposed. In this study, we investigated the potentialities of hybrid membranes made of two distinct components: the rigid fully saturated phospholipid 1,2-dipalmitoyl-*sn-glycero*-3-phosphocholine (DPPC) and the soft copolymer poly(butadiene-*b*-ethyleneoxide) (PBD-*b*-PEO). The objective was to explore the interaction of citrate-coated gold nanoparticles (AuNPs) and the hybrid membrane, aiming at constructing AuNPs-hybrid vesicles suprastructures with controlled and adjustable plasmonic properties. A series of experimental techniques were employed to investigate hybrid free-standing and supported membranes. The results revealed that the incorporation of the copolymer into the lipid membrane promotes AuNPs clustering, demonstrating a distinctive aggregative phenomenon of citrate-coated AuNPs on multidomain membranes. Importantly, we show that the size and morphology of AuNPs clusters can be precisely controlled in non-homogeneous membranes, enabling the formation of hybrid suprastructures with controlled patch properties. These results highlight the potential of lipid-copolymer hybrid

* Corresponding author.
E-mail address: costanza.montis@unifi.it (C. Montis).
[1] JC and AB contributed equally.
[2] Present address: CIC BiomaGUNE Paseo Miramon Donostia, Gipuzkoa, Spain.

https://doi.org/10.1016/j.jcis.2023.10.082
Received 14 July 2023; Received in revised form 16 October 2023; Accepted 17 October 2023
Available online 18 October 2023

membranes for designing functional materials with tailored plasmonic properties, with potential applications in nanomedicine and sensing.

1. Introduction

Lipid assemblies have been extensively studied for decades, and yet fundamental and applied research on lipids remains very active, due to the unique properties of lipid scaffolds, such as high biocompatibility, structural tunability, responsiveness to environmental conditions (temperature, pH). They also exhibit affinity towards hydrophobic or amphiphilic active principles of variable size/charge/polarity, along with easy functionalization. Consequently, lipid assemblies find application in diverse fields including drug delivery, sensing, cosmetics, food science, or as biomimetic systems for fundamental studies on biological membranes [123].

A recent advancement in lipid self-assembly involves the incorporation of amphiphilic copolymers to form hybrid membranes. The inclusion of the copolymer serves multiple purposes: it can enhance the structural stability, as well as the pharmacokinetic properties of lipid vesicles for drug delivery; it can expand the functional properties and chemical tunability of membranes, or induce the formation of multidomain membranes, with lateral phase separated regions, reminiscent of lipid rafts found in cell membranes [4–6]. Combining lipid and copolymer moieties in the same membrane has emerged as a valuable strategy, not only to leverage the advantages of each component, but also to create novel self-assembled soft systems with unique properties arising from the combination of diverse building blocks. In recent years, fundamental studies have focused on understanding the phase behaviour [7–11], self-assembly mechanism, fluidity/dynamics [12] and mechanical properties [13] of copolymer-lipid hybrids. Additionally, investigations into their biological fate [14] when incubated with cells have contributed to the application and translation of hybrid systems. Moreover, applicative studies on hybrid soft assemblies have highlighted copolymer-lipid hybrids as promising candidates for delivering various active principles including small drugs, proteins, macromolecules and nucleic acids [15]. Furthermore, these hybrids have been explored as 2D platforms for the sensors/biosensors development [16,17] and as artificial cells [18].

In this study, we expand the field of lipid-copolymer hybrid systems, improving the fundamental understanding and presenting an original application, which exploits the multidomain nature of copolymer-lipid systems. Copolymer-lipid membranes with phase-separated bidimensional domains contain regions with varying properties in terms of thickness, rigidity, and roughness. By utilizing this feature, we demonstrate the adhesion and clustering of AuNPs on the hybrid membranes, leading to the formation of suprastructures of vesicles and AuNPs, with controlled plasmonic properties.

Recent investigations by our research group and others have addressed the interaction between citrate-coated AuNPs, synthesized using the Turkevich-Frens method, and both synthetic and natural lipid vesicles. Citrate-coated AuNPs[1920] are among the most widely studied inorganic nanoparticles [21222324], due to their ease of synthesis and intriguing optical proprieties resulting from the Surface Plasmon Resonance (SPR) effect [2526]. These studies have shown that AuNPs tend to form clusters on the surface of lipid vesicles when incubated together [2728293031]. Furthermore, this phenomenon strongly depends on the physicochemical and mechanical characteristics of the lipid membrane. Consequently, the plasmonic variations of AuNPs induced by their clustering have been exploited to develop colorimetric assays for characterizing natural and synthetic vesicle dispersions [32333435]. From a nanotechnological perspective, the combination of AuNPs with lipid membranes has been utilized to create smart engineered nanomaterials, such as AuNPs-liposomes suprastructures, serving as biocompatible nanomotors and practical tools for deep-tissue photothermal treatment of immunogenic cancer cells [30,36].

In this work, we expand the investigation of the interfacial interaction between citrate-capped AuNPs and lipid membranes to hybrid membranes composed of the phospholipid 1,2-dipalmitoyl-*sn-glycero*-3-phosphocholine (DPPC) and the copolymer poly(butadiene-*b*-ethyleneoxide) (PBD-*b*-PEO). Both chosen building blocks form in water bilayered membranes which, at r.t., are characterized by significant rigidity for DPPC, and by a softer nature for PBD-*b*-PEO. Recent studies have demonstrated that DPPC and PBD-*b*-PEO self-organize in hybrid bilayered membranes, featuring distinct lipid- and copolymer-rich domains at the nano- and micro-scale. These domains exhibit different fluidity and significant thickness mismatch, resulting in a multidomain, raft-like membrane structure. This structural feature has the potential to strongly influence the interfacial interaction with AuNPs, offering new possibilities for constructing hybrid membrane-AuNPs systems with patch-like properties [37],[51]. To thoroughly explore and understand the mechanistic details of AuNPs-hybrid membrane interaction, we conducted a physico-chemical investigation using quartz crystal microbalance (QCM), confocal laser scanning microscopy (CLSM), UV–Vis spectroscopy and Small-Angle X-rays Scattering (SAXS). Our experimental results reveal the significant role of softer copolymer-rich domains in the interaction, as well as the impact of membrane composition and vesicle concentration on the extent of AuNPs clustering to form controlled AuNPs-hybrid vesicles suprastructures.

Overall, this study enhances our understanding of AuNPs interaction with biomimetic membranes, expanding the current knowledge of complex hybrid membranes with a multidomain nature. From a broader perspective, it contributes to the comprehension of the interaction of inorganic nanoparticles (NPs) and hybrid copolymer-lipid systems, which is crucial for advancing the development of novel and finely controlled engineered nanomaterials, combining the unique properties of inorganic NPs with the physicochemical and mechanical characteristics of hybrid soft copolymer-lipid membranes.

2. Materials and methods

2.1. Materials

DPPC, 1-dipalmitoyl-*sn-glycero*-3-phosphocholine (>99 %), and β-bodipy(2-(4,4-diuoro-5,7-dimethyl-4-bora-3a,4a-diazasindacene-3-pentanoyl, 99 %) were purchased from AVANTI Polar Lipids, Inc. (Alabaster, AL). The copolymer PBD(2500)-*b*-PEO(1500), poly(butadiene-*b*-ethylene oxide, 1,2-addition Bd > 85 %), PBD-*b*-PEO, and the rhodamine-labelled copolymer polybutadiene (Mn = 1200 g/mol)-block-poly(ethylene oxide) (Mn = 600 g/mol, 1,2-addition Bd > 89 %), RhodPBD-*b*-PEO, were provided by Polymer Source. Tetrachloroauric acid ($HAuCl_4$, PM = 393.83 g/mol, ≥ 99.9 %) and sodium citrate ($Na_3C_6H_5O_7$, PM = 258.06 g/mol, ≥ 99.9 %) were provided by Sigma Aldrich (St. Louis, MO). All chemicals were used as received.

2.2. Synthesis of AuNPs

We used the Turkevich-Frens synthesis [20] to obtain a stable dispersion of AuNPs with an approximate diameter of 12 nm. A solution of tetrachloroauric acid was prepared dissolving 20.0 mg in 50 mL of MilliQ water, and then brought to boil under magnetic stirring. A 1 % solution of citric acid (0.153 g in 15 mL of MilliQ water) was added rapidly to the gold solution under agitation. The reaction continued for 15 min and then left cool down at room temperature.

2.3. Preparation of lipid vesicles

DPPC, PBD-*b*-PEO, and hybrid DPPC PBD-*b*-PEO vesicles were prepared with different molar percentages of PBD-*b*-PEO (DPPC PBD-*b*-PEO 5 %, DPPC PBD-*b*-PEO 15 %, DPPC PBD-*b*-PEO 35 %, and DPPC PBD-*b*-PEO 65 %). Lipid and polymer vesicles were produced according to the thin-film hydration method. First, the phospholipid and the copolymer were dissolved in chloroform. Then a thin film was obtained by evaporating the solvent under a N_2 flux and overnight vacuum drying. The films were hydrated with MilliQ water at 50 °C under vigorous stirring reaching a total final lipid and copolymer concentration of 4 mg/mL. The obtained Multilamellar Vesicles (MLVs) were tip sonicated for one minute with a Digital Sonifier Model 450 (Branson, Hampton, NH), provided with a horn tip (diameter 25.4 mm), in intermittent-pulse mode (5 s), with a frequency of 40 kHz (amplitude 30 %). Then, they were subjected to 10 Freeze and Thaw cycles [38]. Finally, to limit the polydispersity[39], the vesicles were extruded through two stacked polycarbonate membranes with pores diameter of 100 nm for 10 times at a temperature of 50 °C. Eventually, unilamellar vesicles (LUV) with a narrow and reproducible size distribution were obtained. The filtration was performed with the Extruder (Lipex Biomembranes, Vancouver, Canada) through Nuclepore membranes.

2.4. Confocal laser scanning microscopy

A Leica CLSM TCS SP8 confocal microscope, operating in inverted mode, with a 63 × 1.3 numerical aperture water immersion objective, was used to image the morphology of polymer and lipid-based surface structures in water excess. β-bodipy(2-(4,4-diuoro-5,7-dimethyl-4-bora-3a,4a-diazasindacene-3-pentanoyl) was used to label DPPC liposomes; the fluorescence of this probe was excited at 488 nm and collected in the 498–530 nm emission range with a Photomultiplier tube (PMT). A rhodamine-labelled copolymer polybutadiene (Mn = 1200 g/mol)-block-poly(ethyne oxide) (Mn = 600 g/mol), RhodPEBD-*b*-PEO was used to label PBD-*b*-PEO polymersomes, employing an excitation wavelength of 561 nm, while the fluorescence was collected in the 571–630 nm range with a PMT detector. The fluorescently-labelled solid-supported bilayers were prepared by vesicles' spontaneous rupture on hydrophilic substrates. SLBs were obtained by adding a 10 mM $CaCl_2$ aqueous solution to a dilute (1 mg/mL) dispersions of vesicles in a 0.1 M NaCl solution and subsequently deposited onto a silicon substrate at T = 50 °C for 30 min. After the deposition, the substrate was washed 15 times with 1 mL of Milli-Q water and then cooled to ambient temperature.

2.5. Quartz crystal microbalance

QCM experiments were executed with a Q-sense Explorer (Q-Sense, Gothenburg, Sweden) instrument equipped with a flux cell containing a quartz-coated sensor with a fundamental resonance of 5 MHz. The active surface of the sensor (≈ 1 cm^2) is covered with a thin film of SiO_2 (≈ 100 nm). The sensors were cleaned before use by washing in pure ethanol and bath sonication for 15 min, nitrogen drying, and finally ozone cleaning for 10 min. The experiments were performed at 41 °C. The sensor was placed in the chamber, and Milli-Q water was injected at a low flow rate (0.1 mL/min). The fundamental resonance frequencies shifts (Δ f) were measured for the odd overtones (3th − 13th). A stable baseline of the different harmonics was ensured before the injection of the vesicles at a low flow rate (0.1 mL/ min). The QCM curves reported are normalized by the overtone number. In the case of rigid films uniformly distributed on the surface of the sensor and thin enough with respect to the weight of the crystal, a linear relation, Sauerbrey equation, connects the absorbed mass (m) and the resonance frequency shift (Δ f):

$$\Delta m = \frac{c}{v}\Delta f \quad (1)$$

with mass sensitivity constant C = 17.7 ng/(cm^2 Hz) for a 5 MHz sensor crystal. The Saurebrey equation was employed to compare the surface mass adsorbed on the sensors for pure and hybrid systems.

2.6. UV–vis spectroscopy

UV–Vis measurements were performed with a Cary 3500 Multizone UV–Vis spectrophotometer. The instrument is equipped with a Xenon lamp, emitting in the range of wavelengths 190–1100 nm. The lamp emits radiations with 250 Hz frequency transmitted through an optic fibre beam to the 8 positions for the samples, each one equipped with its own detector. UV–Vis measurements were performed at room temperature and spectra were acquired in the 300–800 wavelength range.

2.7. Small angle X-ray scattering

Small Angle X-Ray Scattering (SAXS) profiles were measured on AuNPs and hybrid AuNPs-vesicles dispersions using a Xeuss 3.0HR (Xenocs) instrument equipped with a Genix3D (Cu) X-Ray source and a Dectris 1 M Eiger detector. Samples were put in glass capillary tubes of 1.5 mm thickness. Data from each sample were acquired at Sample-Detector (S-D) distances of 450 and 1800 mm for 300 s. The scattering signal was detected in the 0.015 $Å^{-1}$ < Q < 0.6 $Å^{-1}$ Q range. The scattering intensities were normalized with respect to transmission and sample thickness. After data reduction, the contribution of the sample holder and solvent (water) was subtracted from the sample intensity.

To obtain the structure factor S(Q) from the scattering profiles, the scattering intensity of the mixed samples ($I(Q)_{mix}$) was divided by the scattering intensity of neat AuNPs ($I(Q)_{AuNPs}$), as follows:

$$\frac{I(Q)_{mix}}{I(Q)_{AuNPs}} = \frac{P(Q)_{mix}S(Q)_{mix}}{P(Q)_{AuNPs}S(Q)_{AuNPs}}\ S(Q)_{mix}$$

Where the structure factor of bare AuNPs ($S(Q)_{AuNPs}$) is equal to 1, and the form factor of the mixed system ($P(Q)_{mix}$) is equal to the form factor of bare AuNPs ($P(Q)_{mix}$), considering that the P(Q) of the AuNPs cluster does not affect the scattering intensity in the selected Q range [40]. The calculated S(Q) (Fig. 6) shows intensity peaks associated with the interparticle distance ($d = \frac{2\pi}{Q}$).

2.8. Atomic Force microscopy (AFM)

AFM imaging and morphometry was performed as described elsewhere [41]. Briefly, glass coverslips were cleaned for 2 h in a 3:1 H_2SO_4: H_2O_2 solution, rinsed in ultrapure water (Millipore Simplicity), then sonicated for 30′ each in acetone, isopropanol and ultrapure water. Cleaned glass slides were activated with air plasma for 5 min (Pelco Easyglow), then incubated at r.t. for 30′ in a 0.01 mg/ml poly-L-lysine solution in borate buffer at pH 8.5, and finally extensively rinsed with ultrapure water. Samples were incubated for 30′ on functionalized coverslips, then inserted in the AFM fluid cell without drying. AFM imaging was performed on a Multimode8 microscope (Bruker, USA) equipped with a Nanoscope 5 controller and a type J piezoelectric scanner, in PeakForce mode using Scanasyst Fluid + probes (Bruker, USA). Image analysis was performed with Gwyddion [42].

3. Results and discussions

3.1. Lipid-copolymer supported hybrid membranes

Fig. 1a displays the chemical structures of the two building blocks (DPPC for the lipid, PBD-*b*-PEO for the copolymer) of the hybrid membranes. Lipids in water self-assemble to form lamellar structures made of

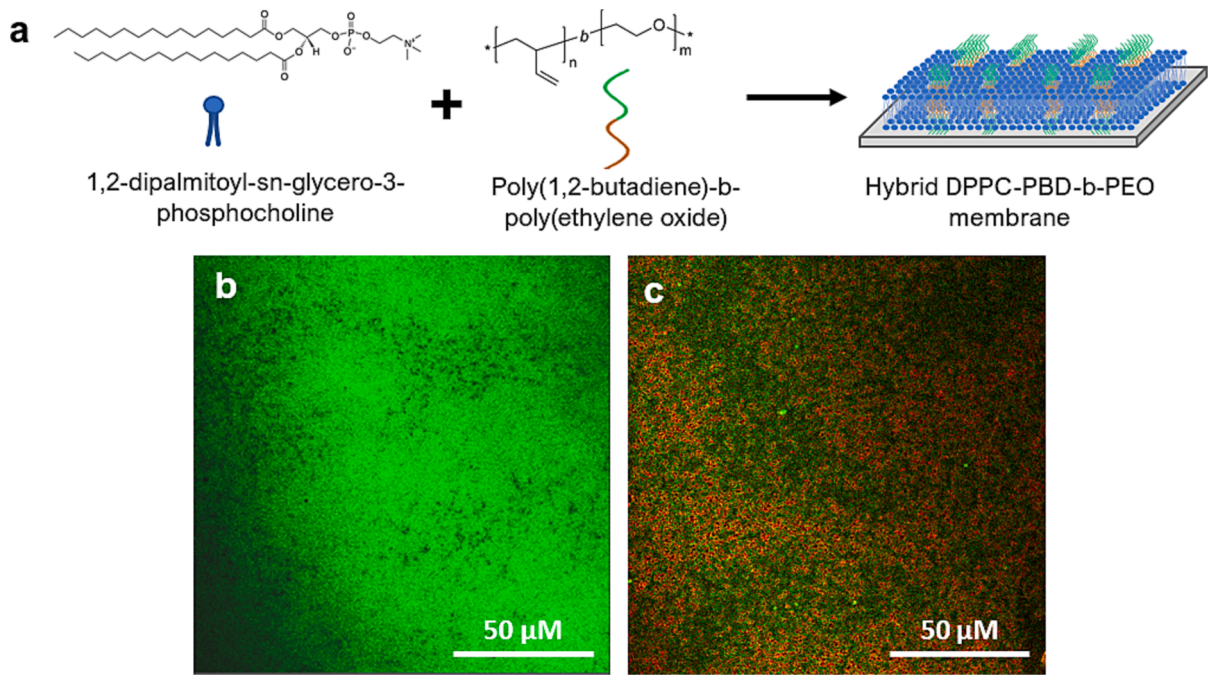

Fig. 1. (a) Chemical structures and illustration of the lipid 1-dipalmitoyl-*sn-glycero*-3-phosphocholine (DPPC), of the copolymer poly(butadiene-*b*-ethylene oxide) (PBD-*b*-PEO) (b). 2D confocal microscopy images of the pure DPPC (c) and the hybrid DPPC PBD-*b*-PEO65%. Merged channels PBD(1200)-*b*-PEO(600) + rhodamine excitation wavelength 561 nm, emission wavelength 571 nm-630 nm (red); β-bodipy excitation wavelength 488 nm, emission wavelength 488 nm-530 nm (green).

lipid bilayers with thickness of around 4 nm, intercalated by aqueous layers. The structure and fluidity of the bilayers depend on the molecular structure of the lipids [43]. DPPC is characterized by a zwitterionic phosphocholine headgroup and by two saturated palmitoyl chains (see Fig. 1). At room temperature, DPPC bilayers possess an organized gel-like structure, with densely packed lipid chains, characterized by a high rigidity. When the temperature is raised above 41 °C, this organized structure becomes liquid crystalline, characterized by different physicochemical features, such as increased softness, permeability, and lateral fluidity. The copolymer PBD-*b*-PEO (Fig. 1a) consists of a biocompatible hydrophilic block (PEO) covalently linked to a hydrophobic moiety; it is characterized by a glass transition temperature below 0 °C (PBD), and by a ratio of hydrophilic to total mass ($f_w = 37$ %) that falls in the range suitable for the design of vesicular structures. As a result, it forms relatively soft polymeric membranes. Once lipids and polymers are blended, two limiting situations are possible depending on the fluidity of the scaffolds. Hybrid lipid-polymer membranes can be formed by mixing the copolymer PBD-*b*-PEO with fluid lipid membranes such as those consisting of the phospholipids 1-palmitoyl-2-oleoyl-*sn-glycero*-3-phosphocholine. (POPC) or 1,2-dioleoyl-*sn-glycero*-3-phosphocholine (DOPC)[44,45]. However, hybrid membranes with lateral phase separation can also be formed by mixing the PBD-*b*-PEO copolymer with rigid lipid membranes. Recent reports have shown that the combination of DPPC with a similar copolymer with a f_w between 29 and 39 % produces hybrid bilayers with phase separated soft, polymer-rich, and rigid, lipid-rich, regions [11,37].

The formation of lipid and hybrid lipid-polymer interfaces onto a hydrophilic substrate was observed via CLSM by labelling the bilayers with two different fluorescent probes: a rhodamine-modified copolymer (RhodPBD-*b*-PEO) and a β-bodipy lipid dye. The selected probes, characterized by well-separated absorption and emission spectra, differ in their affinity to the lipid and copolymer phases. DPPC and DPPC-PBD-*b*-PEO 65 % supported bilayers were formed by spontaneous vesicles' rupture and fusion onto a borosilicate coverglass, according to a well-established protocol [46]. Fig. 1 shows representative CLSM images of the systems. As shown, while the deposition of DPPC vesicles results in the formation of a homogeneous bilayer (Fig. 1b), the inclusion of PBD-PEO induces the formation of a heterogeneous membrane that features clearly distinct lipid (green) and polymer (red) domains (Fig. 1c)[37]. The obtained hybrid system is therefore characterized by a multidomain nature, with copolymer-rich domains (characterized by large thickness, high fluidity/softness and extended polar moieties protruding to the aqueous environment), coexisting with lipid-rich domains (of lower thickness, higher rigidity/stiffness, and low roughness).

3.2. *Interaction of AuNPs with lipid-copolymer supported hybrid membranes*

Once characterized the hybrid copolymer-lipid membrane, we investigated *via* QCM its behaviour when exposed to 12 nm AuNPs synthesized with the Turkevich-Frens method [47]. Pure DPPC and hybrid DPPC-PBD-*b*-PEO65% SLBs (h-SLB) were formed onto the sensor surface at T = 41 °C, close to the gel-liquid crystalline phase transition of DPPC (see Fig. 2a-b). To be noted, under the same experimental conditions PBD-*b*-PEO failed to form a stable film (refer to Figure S6 in the SI), as confirmed by CLSM. Following the formation of the lipid bilayers, the AuNPs dispersion was introduced into the measurement chamber after cooling down the temperature to restore the original gel phase of the DPPC membrane (see Fig. 2c-d) [48].

Fig. 2 reports the resonance frequency shift (Δf) of the quartz crystal sensor, indicative of mass adsorption on the crystal [49], while the measured dissipation factors are reported in Figure S4, (SI). The formation of complete DPPC and DPPC-PBD-*b*-PEO65% bilayers (Fig. 2a and 2b) resulted in frequency shifts of Δf = -30 Hz and Δf = -60 Hz, respectively. Notably, the lower value of Δf observed after the addition of DPPC-PBD-*b*-PEO65% vesicles reflects a higher mass adsorption during the formation of the membrane on the quartz sensor, confirming the successful formation of the hybrid system [37]. While for pure DPPC the measured frequency shift is a clear hallmark of the formation of a single supported lipid bilayer, the doubled frequency shift observed for the hybrid system could be considered as related to the formation of a multi-layered structure. However, in a recent study on a very similar system [37], the combination of QCM-D and ellipsometry data suggested the formation of a single hybrid supported bilayer, and the higher

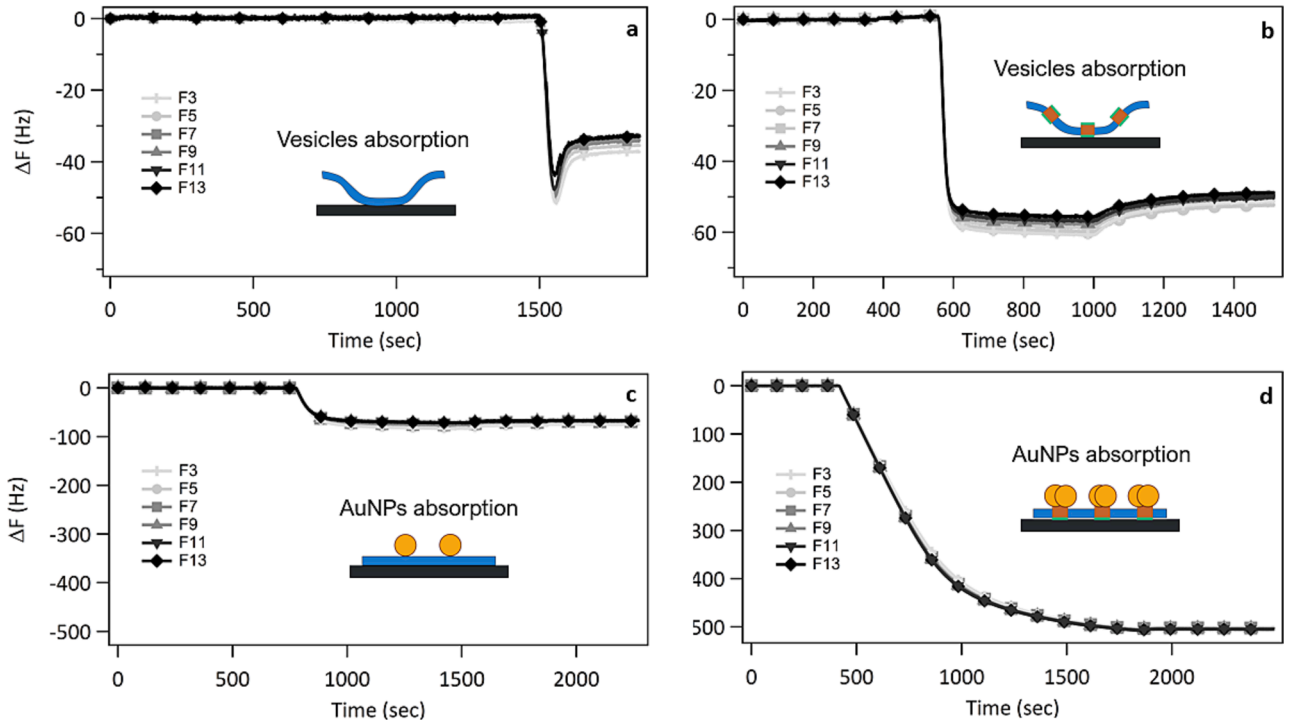

Fig. 2. QCM measurements of the deposition and formation of pure DPPC (a) and hybrid DPPC PBD-*b*-PEO65% (b) supported lipid bilayers at 41 °C. QCM measurements of the deposition and adsorption of AuNPs onto pure DPPC (c) and hybrid DPPC PBd-*b*-PEO65% (d) SLB at room temperature (25 °C). Frequency variation measured for 3th, 5th, 7th, 9th, 11th and 13th harmonics.

adsorbed mass was attributed to the inclusion of the copolymer moiety in the membrane, characterized by an extended and highly hydrated polar headgroup. Fig. 2c and 2d show that the injection of AuNPs results in an increase of the absolute value of the frequency shifts (Δf = -70 Hz for the deposition of AuNPs on pure DPPC SLB, Δf = -500 Hz on the hybrid SLB), thereby indicating the adsorption of AuNPs on the membrane. Remarkably, the larger Δf observed for the hybrid SLB highlights the significantly higher affinity of AuNPs for the hybrid bilayer. Considering for both cases a purely elastic regime, to quantitatively assess the interaction between AuNPs and the membranes, the total adsorbed mass of AuNPs was calculated using the Sauerbrey equation (see equation (1) in Material and Methods)[50]. The calculated adsorbed mass on the DPPC PBD-*b*-PEO65% bilayer is about 9000 ng/cm^2, while only about 1200 ng/cm^2 adhere to the DPPC SLB. These results point out that the inclusion of the polymer into the lipid membrane promotes the adhesion/adsorption of AuNPs on the membrane. Interestingly, in a previous study we observed that the adsorption of citrate-coated AuNPs on a supported lipid bilayer was limited, even in the case of a membrane in the liquid crystalline phase, such as POPC [28]. We attributed the limited ability of the supported POPC membrane to establish favourable interfacial interactions with citrate-coated AuNPs to the high bending rigidity of the membrane anchored to a solid support. The obtained results highlight that the inclusion of PBD-*b*-PEO copolymer in the rigid DPPC lipid membrane enhances the ability of the membrane to attract AuNPs. This effect can be likely attributed to a combination of factors: firstly, the mismatch in thickness between the lipid and the copolymer components prevents the strong coupling of the whole h-SLB to the solid support, thereby increasing the ability of the bilayer to interact with the AuNPs; secondly, the macromolecular nature of the PBD-PEO copolymer might extend the effective interfacial area of the hybrid SLB, ultimately enhancing the adhesion of AuNPs on the membrane. However, it is important to note that the overall "softer" nature of the polymer component compared to DPPC may also contribute to these observed effects.

3.3. Characterization of lipid-copolymer hybrid vesicles

To investigate the influence of polymer inclusion on the elastic properties of free-standing nanosized vesicles, we employed an AFM-morphometry-based assay, previously exploited for the nanomechanical assessment of synthetic and natural vesicles [5253]. Briefly, intact DPPC, DPPC PBD-*b*-PEO65%, and PBD-*b*-PEO vesicles were deposited on a poly-L-lysine functionalized glass substrate, and liquid AFM imaging was performed to determine their individual contact angles (CA), which are quantitatively related to their stiffness values. Higher CAs correspond to higher mechanical stiffnesses. As shown in Fig. 3, incubating DPPC and DPPC-PBD-*b*-PEO65% vesicles on the glass substrates resulted in the adhesion of intact vesicles having average CAs of 97°±11° and 92°±10°, respectively. These observations suggest that the copolymer inclusion in the lipid bilayer induces an overall slight decrease in stiffness. In contrast, when attempting to deposit pure PBD-*b*-PEO vesicles under the same conditions, their rupture occurred after adhesion, thus leaving on the substrate discrete SLB patches, putatively corresponding to the previously intact individual vesicles. As SLB patches lack a CA, it is impossible to directly compare the stiffness of pure polymersomes with liposomes and hybrid vesicles *via* this method; however, the different percentages of intact adhered vesicles in the three cases suggest that their response to mechanical stresses is highly different. Specifically, DPPC vesicles adsorb intact on the substrate, PBD-*b*-PEO pure polymersomes spontaneously fuse, forming supported bilayer patches, and hybrids show an intermediate behaviour (Fig. 3), in line with the bending rigidity data of similar lipid and polymeric scaffolds [18].

3.4. Interaction of AuNPs with pure lipid and copolymer vesicles

To gain a deeper understanding of how the mechanical differences observed in AFM experiments affect the interaction between free-standing vesicles and AuNPs, we performed UV–Vis experiments. We monitored the changes in the optical properties of AuNPs after

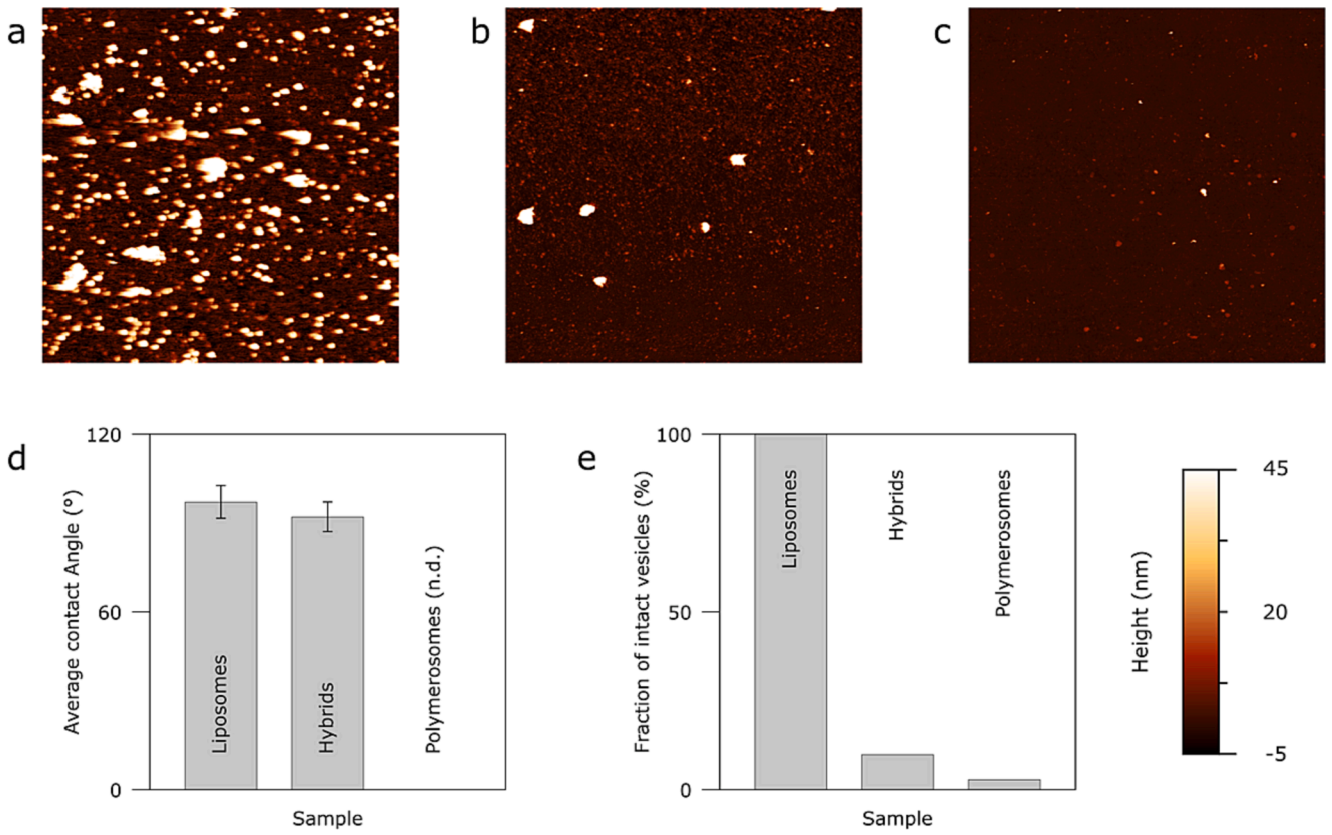

Fig. 3. Liquid AFM images of DPPC (a), DPPC PBD-*b*-PEO65% (b) and PBD-*b*-PEO (c) SLB. Comparison of contact angle (d) and of fraction of intact vesicles (e) between pure DPPC, DPPC PBD-*b*-PEO65% and hybrid vesicles.

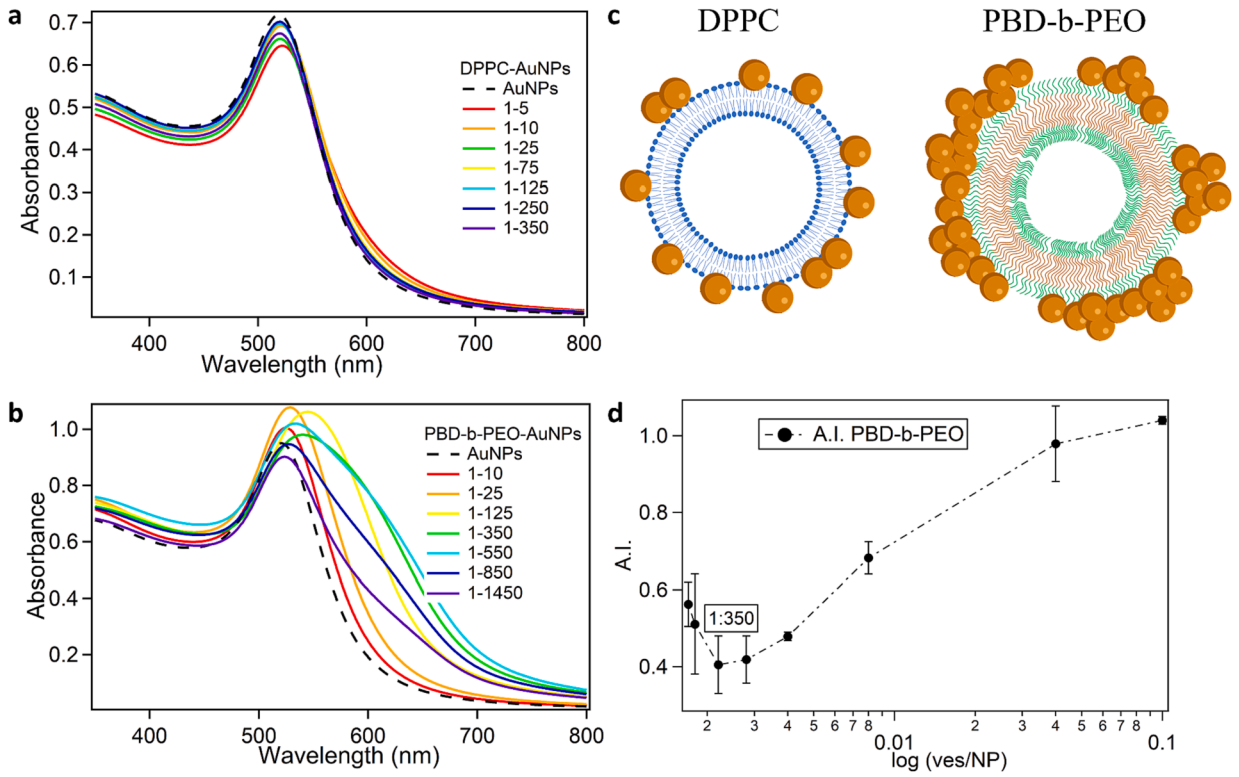

Fig. 4. UV–Vis spectra of 300 μL of 9.93 × 10^{-9} M AuNPs were incubated with 10 μL of a) DPPC and b) PBD-*b*-PEO vesicles in the following vesicles/NPs ratios: 1/5, 1/10, 1/25, 1/50, 1/75, 1/125, 1/150, 1/200, 1/250, 1/350, 1/450, 1/550, 1/850, 1/1250, and 1/1450. Schematic illustration of AuNPs clustering on the vesicle membrane (c) and A.I. vs log(vesicle/NP) plot for PBD-*b*-PEO (d). A.I. values are the average of three measurements on different batches.

incubation with 100 nm vesicles at different PBD-*b*-PEO molar percentages (DPPC, DPPC PBD-*b*-PEO5%, DPPC PBD-*b*-PEO15%, DPPC PBD-*b*-PEO35%, DPPC PBD-*b*-PEO65%, PBD-*b*-PEO) and vesicle/NPs ratios (1/5, 1/10, 1/25, 1/50, 1/75, 1/125, 1/150, 1/200, 1/250, 1/350, 1/450, 1/550, 1/850, 1/1250, and 1/1450).

Fig. 4a illustrates the evolution of the plasmon peak of AuNPs after incubation with DPPC at various vesicle/NPs ratios. It is evident that the interaction between DPPC vesicles and AuNPs has negligible effects on the plasmonic peak, in accordance with previous literature findings [2729]. We hypothesize that the rigid nature of DPPC membranes inhibits the clustering of AuNPs on the lipid surface, resulting in single particle adhesion (as shown in Fig. 4c). In contrast, incubating AuNPs with PBD-*b*-PEO polymersomes leads to a significant change in the colour of the gold dispersion from red to purple-blue, accompanied by a broadening of the plasmonic peak (Fig. 4b). This experimental evidence indicates plasmon coupling of proximal NPs and confirms the clustering of AuNPs on the vesicle membrane (as depicted in Fig. 4c). The interaction between citrate-coated AuNPs and polymer vesicles has been rarely investigated in previous studies [52]. In recent studies, by combining experimental [28] and computational tools [29] we proved that citrate-coated AuNPs interact with soft lipid vesicles of POPC or DOPC through a phosphocholine-citrate ligand exchange process occurring at the nano-bio interface. The adhesion of AuNPs to the lipid surface triggers the fast release of the exchangeable citrate moieties from AuNPs surface, ultimately driving the membrane templated clustering of AuNPs on the vesicles surface. Remarkably, the results here shown demonstrate that AuNPs interact with soft PBD-*b*-PEO polymersomes and cluster on them, similarly to what is observed with soft lipid vesicles. This finding suggests that the exchangeability of citrate capping agent and the vesicles' stiffness are the main factors at play in driving AuNPs clustering on vesicles, and that, interestingly, the ligand exchange between AuNPs citrate coating and the polar headgroups of the membrane components occurs both for lipid and for copolymer systems. Probably, as already hypothesized [52], the affinity for PBD-*b*-PEO hydrophilic PEO chains promotes AuNPs adhesion and ligand exchange at the nano-bio interface, ultimately leading to the clustering of AuNPs on PBD-*b*-PEO vesicles. However, taking into account the polymer nature of the vesicles, more complex effects with respect to lipid vesicles, for instance depletion forces, could be also at play [53,54].

An inspection of the UV–Vis absorbance curves obtained at different PBD-*b*-PEO vesicle/AuNPs ratios (Fig. 4b), reveals an interesting trend. For high vesicle/AuNPs fraction, a decrease in the vesicle/AuNPs ratio leads to a progressive broadening of the plasmonic band, until a maximum. Further increasing the number of NPs per vesicle results in the restoration of the original plasmonic properties, highlighting a non-monotonic behaviour in the AuNPs aggregation extent with vesicle concentration increase. To quantify this behaviour, we introduce an aggregation index (A.I.), which serves as a descriptor of AuNPs clustering [32]:

$$A.I. = \frac{Abs_{max} - Abs_{600}}{\Delta\lambda} \quad (2)$$

Where Abs_{max} is the absorbance of the AuNPs characteristic peak, generally located at about 520 nm, Abs_{600} is the absorbance at 600 nm, typical of AuNPs clusters, and $\Delta\lambda$ is the difference between the two wavelengths. The calculated A.I.s were then normalized for the one calculated for the isolated AuNPs; consequently, the normalized A.I. value of neat AuNPs is equal to 1, and the higher the plasmonic variations (and consequently the AuNPs aggregation), the lower is the aggregation index.

In Fig. 4d, we present an analysis from Fig. 4b UV, specifically displaying the estimated A.I. values of AuNPs incubated with PBD-*b*-PEO vesicles as a function of the AuNPs/vesicles ratio. As anticipated, the relationship between the AuNPs aggregation extent and the AuNPs/vesicles ratio is non-monotonic. When the AuNPs/vesicles ratio is low, increasing the number of AuNPs per vesicle leads to a higher clustering extent, resulting in a decrease in A.I.. Conversely, at high AuNPs/vesicles ratios, we can hypothesize that the vesicles surface becomes saturated by AuNPs. Therefore, increasing the AuNPs number per vesicle results in a higher number of free AuNPs dispersed in solution compared to the clustered ones, ultimately causing a decrease in the observed plasmonic shift.

3.5. Interaction of AuNPs with lipid-copolymer hybrid vesicles

After investigating the interaction between AuNPs and pure DPPC or pure PBD-*b*-PEO vesicles, we proceeded to study the interaction of AuNPs with hybrid vesicles (h-vesicles) containing varying amounts of PBD-*b*-PEO in relation to DPPC. UV–Vis spectroscopy was employed to monitor the changes in plasmonic properties at different AuNPs/h-vesicles molar ratios. Fig. 5 displays some representative UV–Vis traces obtained for AuNPs incubated with (a) DPPC PBD-*b*-PEO5%, (b) DPPC PBD-*b*-PEO15%, (c) DPPC PBD-*b*-PEO35%, (d) DPPC PBD-*b*-PEO65% vesicles, at various AuNPs/h-vesicles ratios.

Interestingly, we observed a similar behaviour for all the investigated systems reminiscent of what observed for the pure copolymer vesicles. Specifically, the presence of PBD-*b*-PEO within DPPC membranes promoted the clustering of AuNPs on the hybrid vesicles, confirming that the copolymer acts as a "sticky region" that attracts AuNPs and determines the formation of AuNPs aggregates. Additionally, similar to the findings for PBD-*b*-PEO vesicles, the aggregation extent has a non-monotonic relation with AuNPs/h-vesicles ratio (see Figure S7 the A.I. vs AuNPs/h-vesicles ratio traces obtained for the different hybrid systems).

To gain further insights into the specific role of PBD-*b*-PEO in inducing AuNPs clustering, we examined the parameter $(AuNPs/vesicles)_{max}$ which represents the value of AuNPs/vesicles ratio corresponding to the maximum extent of AuNPs clustering from Fig. 4d. In other words, it indicates the amount of AuNPs per vesicle at which the vesicle surface becomes saturated by AuNPs clusters. Remarkably, when $(AuNPs/vesicles)_{max}$ is analyzed as a function of PBD-*b*-PEO percentage compared to DPPC in the hybrid vesicles, a clear interdependence between the two parameters emerges. As Illustrated in Fig. 6, we propose that the increase of PBD-*b*-PEO in the vesicle leads to an average increase of PBD-*b*-PEO patches (in number and size) in DPPC vesicles, thus increasing the sticky regions within the vesicles where AuNPs can adhere. This effect is particularly pronounced at low PBD-*b*-PEO concentrations, resulting in an initial steep increase of $(AuNPs/vesicles)_{max}$ as a function of PBD-*b*-PEO molar percentage (Fig. 6). For high PBD-*b*-PEO amounts, it can be hypothesized that the finite size of the vesicles and the electrostatic repulsion between separate clusters slow down AuNPs clustering.

The UV–vis spectroscopic properties of AuNPs aggregates can be attributed to different factors, including the polydispersity of the aggregates in terms of size and mutual distance between AuNPs as well as the presence of freely dispersed AuNPs. To gain further insights into the structure of AuNPs aggregates on the hybrid vesicles, we performed SAXS experiments. The experimental conditions were carefully adjusted to minimize the contribution of the vesicles to the scattering signal, allowing us to obtain SAXS profiles solely from AuNPs in their dispersed or clustered forms (see SI). Fig. 7a presents the S(Q) of the aggregates (see the Material and Methods section), from which the interparticle distances between AuNPs in the aggregates were extrapolated. Interestingly, for each vesicle formulation, the minimum interparticle distance observed, corresponding to the mean AuNP-AuNP distance in the aggregates at the maximum AuNPs extent, remains constant (≈11.6 nm). This value is consistent with the AuNPs size, indicating that most AuNPs are in contact with each other within the aggregates. The attainment of this minimum AuNP-AuNP spacing occurs for vesicle/AuNPs ratios characterized by the highest plasmonic variations. Importantly, as the number of copolymer patches in the vesicles is

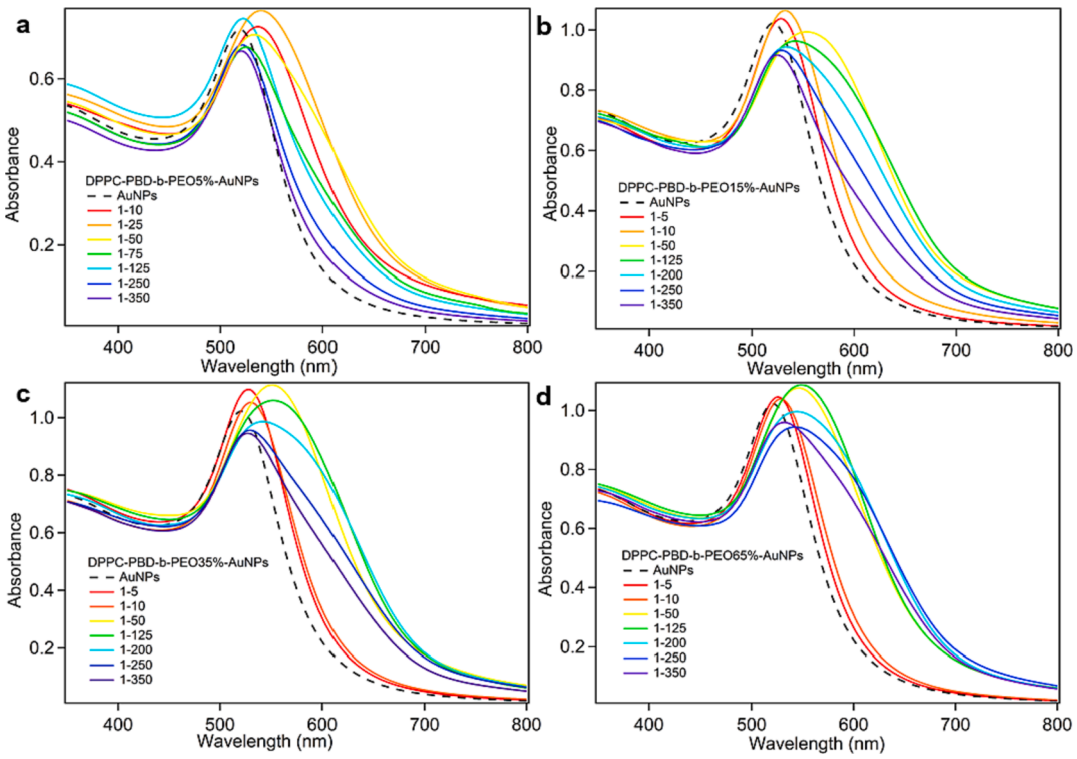

Fig. 5. UV–Vis spectra of 300 μL of 9.93×10^{-9} M AuNPs were incubated with 10 μL of vesicles in the following vesicles/NPs ratios: 1/5, 1/10, 1/25, 1/50, 1/75, 1/125, 1/150, 1/200, 1/250, 1/350, 1/450, 1/550, 1/850, 1/1250, and 1/1450. a) A.I. vs log(vesicle/NP) plot for DPPC PBD-*b*-PEO5%, b) A.I. vs log(vesicle/NP) plot for DPPC PBD-*b*-PEO15%, c) A.I. vs log(vesicle/NP) plot for DPPC PBD-*b*-PEO35%, d) A.I. vs log(vesicle/NP) plot for DPPC PBD-*b*-PEO65%, e) A.I. vs log(vesicle/NP) plot for PBD-*b*-PEO.

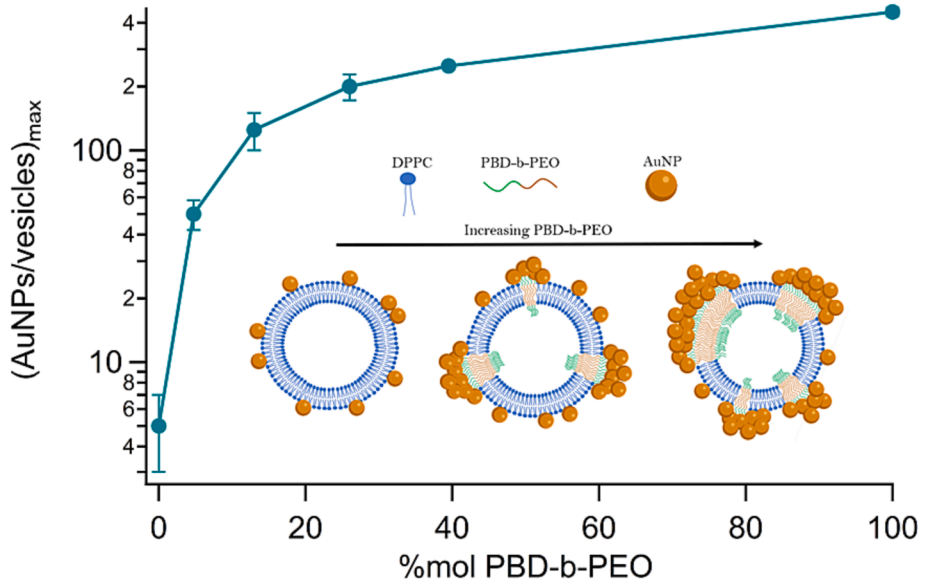

Fig. 6. Amount of AuNPs per vesicle corresponding to the vesicles surface saturation by AuNPs clusters ($(AuNPs/vesicles)_{max}$) for each hybrid vesicle composition. AuNPs/vesicles values are determined as the average of three measurements on different batches.

further reduced, the intensity of the S(Q) peaks decreases without affecting their position. This suggests that the interparticle distance between AuNP in the aggregates, which has been previously demonstrated to depend on the stiffness of the vesicle, remains invariant [32].

In the low Q region, the power-law trend of the scattering profiles provides insights into the dimensionality of the AuNPs clusters, and the slope of log I(Q) vs log (Q) can be associated with their fractal dimensions (d_f)[55,56]. The fractal dimension increases with increasing compactness. Fig. 7b presents the SAXS profiles of AuNPs-hybrid vesicles obtained at the AuNPs/h-vesicles ratio corresponding to the maximum extent of aggregation as determined by the UV–vis data, for the different DPPC-PBD-*b*-PEO formulations. Interestingly, the maximum slope value (see Table S17) exhibits an increase with the polymer content, ranging from 0.5 for pure DPPC liposomes to 2.9 for pure PBD-*b*-PEO vesicles. This finding highlights that an increased amount of PBD-*b*-PEO leads to the formation of more compact gold

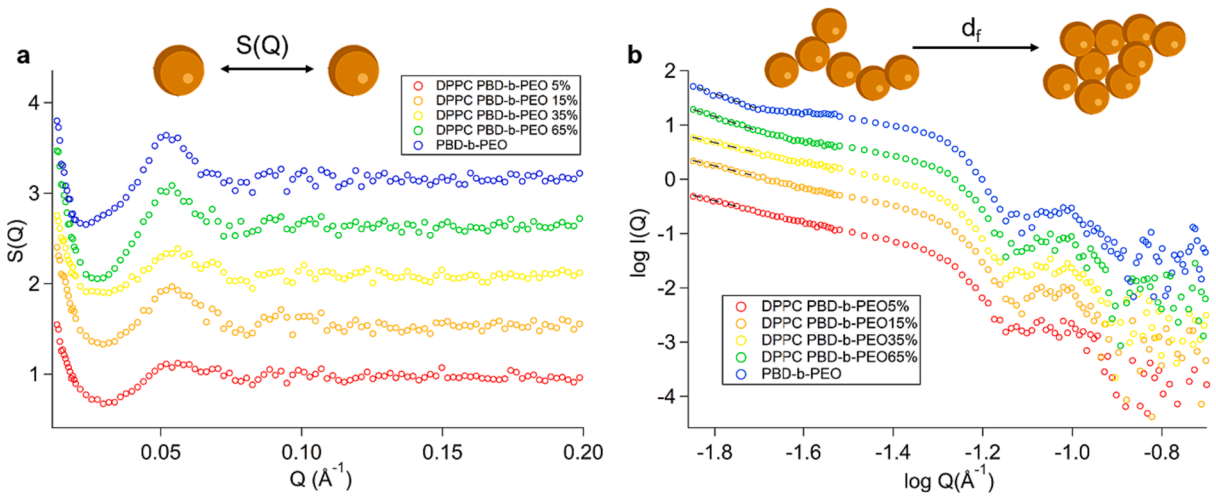

Fig. 7. Structure factors (S(Q)) evaluated after 10 min of incubation of 300 μL AuNPs 9.93 nM with DPPC-PBD-*b*-PEO5%, DPPC-PBD-*b*-PEO15%, DPPC-PBD-*b*-PEO35%, DPPC-PBD-*b*-PEO65% and PBD-*b*-PEO vesicles at vesicles surface saturation by AuNPs clusters ratio ($(AuNPs/vesicles)_{max}$) for each hybrid vesicle composition, by dividing the $I(Q)_{mix}$ by $I(Q)_{AuNPs}$. The correlation peaks are related to the AuNP-AuNP center-to-center interparticle distances (a). Log – log SAXS profiles of AuNPs/vesicles hybrids collected for each hybrid vesicle composition at the $(AuNPs/vesicles)_{max}$ (b). Dashed black lines indicate the linear fittings of the low Q region.

aggregates.

Overall, the SAXS data suggest that the adhesion and clustering of AuNPs on the hybrid membrane are primarily due to the presence of soft polymer-rich regions with low stiffness within the hybrid vesicles. The softness of the polymer-rich regions appears to be independent on the PBD-*b*-PEO percentage within the h-vesicles, resulting in AuNPs clusters with similar interparticle distances regardless of the PBD-*b*-PEO content. On the other hand, the percentage of PBD-*b*-PEO in the vesicles controls the extension of "sticky regions" within the vesicles, leading to the formation of AuNPs clusters of different compactness, ultimately influencing their plasmonic properties.

3.6. AuNPs-hybrid vesicles suprastructures: Mechanistic understanding and structural control

Taking all the data into consideration, we can rationalize the phenomenon of AuNPs clustering on hybrid copolymer-lipid vesicles. Specifically, we observe that AuNPs aggregation is strongly inhibited on the DPPC rigid membrane, irrespective of the number of vesicles present. However, the introduction of soft polymeric domains within the vesicles induces a significant change in the aggregation behaviour of AuNPs, promoting selective aggregation on the copolymer patches present on the vesicles. Two parameters can be utilized to control the size and compactness of these patches. Firstly, the total concentration of vesicles (specifically, the AuNPs/vesicles ratio) governs the available surface area for AuNPs aggregation. Thus, decreasing h-vesicles/AuNPs ratio

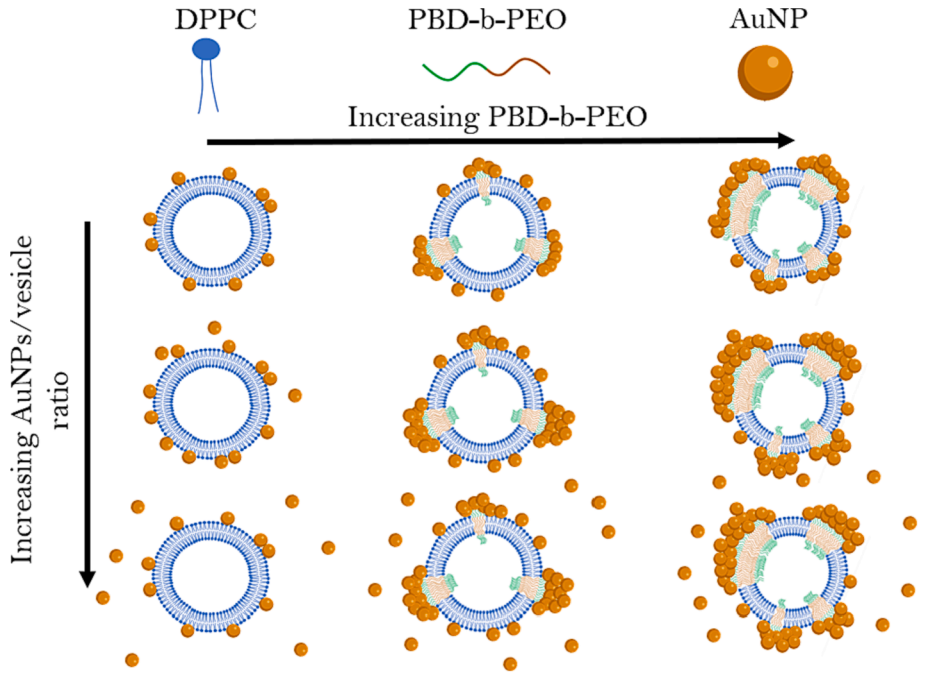

Fig. 8. Illustration of AuNPs aggregation on vesicles depending on the polymer content and on the vesicles concentration.

leads to a non-monotonic trend of AuNPs aggregation (see the scheme in Fig. 8, vertical axis). Secondly, the relative percentage of PBD-*b*-PEO in the formulation influences the number and size of polymer-rich "sticky patches" within the hybrid membrane, thereby controlling the formation of clustered AuNPs on the vesicles' surface (see the scheme in Fig. 8, horizontal axis).

Reasonably, we can assume that the maximum aggregation of AuNPs in each sample corresponds to the saturation of the membrane by AuNPs, which, in turn, depends on the extension of the soft polymeric domains. Further decreasing in vesicles/AuNPs ratio leads to a larger number of dispersed NPs in solution, restoring the original plasmonic and scattering features. In line with this assumption, the saturation of the hybrid vesicles is controlled by the vesicles/AuNPs ratio, while the compactness of gold aggregates can be controlled by adjusting the polymer/lipid ratio in the vesicle formulations.

4. Conclusions

In this study we investigated the interaction between hybrid copolymer-lipid membranes and citrate-coated gold nanoparticles (AuNPs), aiming at creating a suprastructure with tunable and controlled plasmonic characteristics using self-assembly steps.

Firstly, we successfully formed hybrid membranes composed of 1,2-dipalmitoyl-*sn-glycero*-3-phosphocholine (DPPC) and poly(butadiene-*b*-ethyleneoxide) (PBD-*b*-PEO), characterized by a multidomain nature where soft, rough, and thick polymer-rich regions coexist with rigid, smoother, and thinner lipid-rich regions. Atomic Force Microscopy (AFM) analysis demonstrated significantly different mechanical responses between pure DPPC and PBD-*b*-PEO vesicles, while the hybrid vesicles exhibited intermediate properties. Upon interaction with AuNPs, a combination of UV–vis spectroscopy and Small-Angle X-ray Scattering (SAXS) data revealed that pure soft PBD-*b*-PEO vesicles facilitated the clustering of AuNPs on the membrane, whereas this effect was negligible for stiff DPPC vesicles. Regarding lipid-copolymer hybrid vesicles, our results demonstrated that the inclusion of the soft PBD-*b*-PEO copolymer in DPPC assemblies induced the formation of AuNPs clusters, likely within the soft polymer-rich regions of the membrane, which act as "sticky domains" promoting the adhesion and clustering of AuNPs. SAXS and UV–vis analyses revealed that two main parameters govern the size and compactness of AuNPs on the hybrid vesicles: (i) the ratio between AuNPs and hybrid vesicles and (ii) the relative percentage of copolymer with respect to lipid within the vesicles. These factors represent independent variables that can be leveraged to modulate the size of AuNPs patches on the hybrid vesicles, ultimately enabling the tuning of their plasmonic properties.

The results here shown contribute to the understanding of the interaction between citrated AuNPs and membranes, extending the current knowledge on lipid [29] and copolymer membranes [52] to more complex hybrid systems; in particular, lateral phase separation in multidomain lipid/copolymer hybrid membranes was highlighted as a key factor to drive the spontaneous patched clustering of the citrated AuNPs; in addition, specific and simple control parameters (i.e., AuNPs/vesicles ratio and lipid/copolymer ratio in the formulation) were identified to regulate the spontaneous self-assembly of the AuNPs on the target membrane at will, to ultimately tune the colloidal and plasmonic properties of the resulting adduct.

Overall, our findings will contribute to provide fundamental knowledge for the design of inorganic–organic hybrid materials with tailored characteristics built-up through simple self-assembly.

CRediT authorship contribution statement

Jacopo Cardellini: Investigation, Methodology, Formal analysis, Writing – original draft. **Arianna Balestri:** Investigation, Methodology, Formal analysis, Writing – original draft. **Luca Comparini:** Investigation, Formal analysis. **Barbara Lonetti:** Investigation, Writing – review & editing. **Marco Brucale:** Investigation, Writing – review & editing. **Francesco Valle:** Investigation, Writing – review & editing. **Debora Berti:** Conceptualization, Methodology, Supervision, Project administration, Funding acquisition, Writing – review & editing. **Costanza Montis:** Conceptualization, Investigation, Methodology, Formal analysis, Supervision, Writing – review & editing.

Declaration of Competing Interest

The authors declare that they have no known competing financial interests or personal relationships that could have appeared to influence the work reported in this paper.

Data availability

Data will be made available on request.

Acknowledgements

The authors acknowledge MIUR-Italy ("Progetto Dipartimenti di Eccellenza 2018–2022, ref B96C1700020008" allocated to the Department of Chemistry "Ugo Schiff") and the Center for Colloid and Surface Science (CSGI) for economic support.

Appendix A. Supplementary data

Supplementary data to this article can be found online at https://doi.org/10.1016/j.jcis.2023.10.082.

References

[1] C. Montis, D. Maiolo, I. Alessandri, P. Bergese, D. Berti, Interaction of nanoparticles with lipid membranes: a multiscale perspective, Nanoscale 6 (12) (2014) 6452–6457, https://doi.org/10.1039/C4NR00838C.
[2] A.K. Sachan, R.K. Harishchandra, C. Bantz, M. Maskos, R. Reichelt, H.-J. Galla, High-Resolution Investigation of Nanoparticle Interaction with a Model Pulmonary Surfactant Monolayer, ACS Nano 6 (2) (Feb. 2012) 1677–1687, https://doi.org/10.1021/nn204657n.
[3] C. Montis, et al., Biogenic supported lipid bilayers as a tool to investigate nano-bio interfaces, J. Colloid Interface Sci. 570 (June 2019) (2020) 340–349, https://doi.org/10.1016/j.jcis.2020.03.014.
[4] S.K. Patra, Dissecting lipid raft facilitated cell signaling pathways in cancer, Biochim. Biophys. Acta - Rev. Cancer 1785 (2) (2008) 182–206, https://doi.org/10.1016/j.bbcan.2007.11.002.
[5] S.-W. Hu, C.-Y. Huang, H.-K. Tsao, Y.-J. Sheng, Hybrid membranes of lipids and diblock copolymers: From homogeneity to rafts to phase separation, Phys. Rev. E 99 (1) (Jan. 2019), 012403, https://doi.org/10.1103/PhysRevE.99.012403.
[6] M. Schulz, W.H. Binder, Mixed Hybrid Lipid/Polymer Vesicles as a Novel Membrane Platform, Macromol. Rapid Commun. 36 (Dec. 2015) 2031–2041.
[7] J.A. Hammons, et al., Decoupling copolymer, lipid and carbon nanotube interactions in hybrid, biomimetic vesicles, Nanoscale 12 (11) (2020) 6545–6555, https://doi.org/10.1039/c9nr09973e.
[8] R.M. Perera, et al., Nanoscale Lipid/Polymer Hybrid Vesicles: Effects of Triblock Copolymer Composition and Hydrophilic Weight Fraction, ACS Appl. Polym. Mater. 4 (12) (2022) 8858–8868, https://doi.org/10.1021/acsapm.2c01272.
[9] E. Brodszkij, et al., Membrane composition of polymer-lipid hybrid vesicles, Appl. Mater. Today 29 (April) (2022), https://doi.org/10.1016/j.apmt.2022.101549.
[10] Y. Miele, et al., Hybrid giant lipid vesicles incorporating a PMMA-based copolymer, Biochim. Biophys. Acta - Gen. Subj. 1865 (4) (2021), 129611, https://doi.org/10.1016/j.bbagen.2020.129611.
[11] N. Hamada, S. Gakhar, M.L. Longo, Hybrid lipid/block copolymer vesicles display broad phase coexistence region, Biochim. Biophys. Acta - Biomembr. 1863 (4) (Apr. 2021), 183552, https://doi.org/10.1016/j.bbamem.2021.183552.
[12] G. Bello, F. Cavallini, L.A. Dailey, E.K. Ehmoser, Supported polymer/lipid hybrid bilayers formation resembles a lipid-like dynamic by reducing the molecular weight of the polymer, Biochim. Biophys. Acta - Biomembr. 1863 (1) (2021), 183472, https://doi.org/10.1016/j.bbamem.2020.183472.
[13] M. Fauquignon, E. Ibarboure, J.F. Le Meins, Membrane reinforcement in giant hybrid polymer lipid vesicles achieved by controlling the polymer architecture, Soft Matter 17 (1) (2021) 83–89, https://doi.org/10.1039/d0sm01581d.
[14] E. Brodszkij, I.N. Westensee, M. Bertelsen, N. Gal, T. Boesen, B. Städler, Polymer–Lipid Hybrid Vesicles and Their Interaction with HepG2 Cells, Small 16 (27) (2020) 1–9, https://doi.org/10.1002/smll.201906493.
[15] S. Khan, J. McCabe, K. Hill, P.A. Beales, Biodegradable hybrid block copolymer – lipid vesicles as potential drug delivery systems, J. Colloid Interface Sci. 562 (2020) 418–428, https://doi.org/10.1016/j.jcis.2019.11.101.

[16] S. Di Leone, et al., Polymer-Lipid Hybrid Membranes as a Model Platform to Drive Membrane-Cytochrome c Interaction and Peroxidase-like Activity, J. Phys. Chem. B 124 (22) (2020) 4454–4465, https://doi.org/10.1021/acs.jpcb.0c02727.
[17] E.A. Schafer, E. Davis, Z. Manzer, S. Daniel, J. Rivnay, Hybrid Supported Lipid Bilayers for Bioinspired Bioelectronics with Enhanced Stability, ACS Appl. Mater. Interfaces 15 (20) (2023) 24638–24647, https://doi.org/10.1021/acsami.3c01054.
[18] Y.K. Go, C. Leal, Polymer-Lipid Hybrid Materials, Chem. Rev. 121 (22) (2021) 13996–14030, https://doi.org/10.1021/acs.chemrev.1c00755.
[19] G. Frens, Controlled Nucleation for the Regulation of the Particle Size in Monodisperse Gold Suspensions, Nat. Phys. Sci. 241 (1973) 20–22, https://doi.org/10.1038/physci241020a0.
[20] J. Turkevich, P.C. Stevenson, J. Hillier, A study of the nucleation and growth processes in the synthesis of colloidal gold, Discuss. Faraday Soc. 11 (1951) 55–75, https://doi.org/10.1039/DF9511100055.
[21] S.B. Yaqoob, R. Adnan, R.M. Rameez Khan, M. Rashid, Gold, Silver, and Palladium Nanoparticles: A Chemical Tool for Biomedical Applications, Front. Chem. 8 (June) (2020) 1–15, https://doi.org/10.3389/fchem.2020.00376.
[22] E.C. Dreaden, A.M. Alkilany, X. Huang, C.J. Murphy, M.A. El-Sayed, The golden age: Gold nanoparticles for biomedicine, Chem. Soc. Rev. 41 (7) (2012) 2740–2779, https://doi.org/10.1039/c1cs15237h.
[23] S. Balakrishnan, F.A. Bhat, A. Jagadeesan, Applications of gold nanoparticles in cancer, Biomed. Eng. Concepts, Methodol. Tools, Appl. (2017) 780–808, https://doi.org/10.4018/978-1-5225-3158-6.ch035.
[24] A.M. Alkilany, S.E. Lohse, C.J. Murphy, The gold standard: Gold nanoparticle libraries to understand the nano-bio interface, Acc. Chem. Res. 46 (3) (2013) 650–661, https://doi.org/10.1021/ar300015b.
[25] V. Amendola, R. Pilot, M. Frasconi, O.M. Maragò, M.A. Iatì, Surface plasmon resonance in gold nanoparticles: A review, J. Phys. Condens. Matter 29 (20) (2017), https://doi.org/10.1088/1361-648X/aa60f3.
[26] A.H.R. Koch, et al., Probing Nanoparticle/Membrane Interactions by Combining Amphiphilic Diblock Copolymer Assembly and Plasmonics, J. Phys. Chem. B 124 (5) (2020) 742–750, https://doi.org/10.1021/acs.jpcb.9b10469.
[27] K. Sugikawa, T. Kadota, K. Yasuhara, A. Ikeda, Anisotropic Self-Assembly of Citrate-Coated Gold Nanoparticles on Fluidic Liposomes, Angew. Chemie - Int. Ed. 55 (12) (2016) 4059–4063, https://doi.org/10.1002/anie.201511785.
[28] C. Montis, et al., Shedding light on membrane-templated clustering of gold nanoparticles, J. Colloid Interface Sci. 573 (Aug. 2020) 204–214, https://doi.org/10.1016/j.jcis.2020.03.123.
[29] J. Cardellini, et al., Membrane Phase Drives the Assembly of Gold Nanoparticles on Biomimetic Lipid Bilayers, J. Phys. Chem. C 126 (9) (2022) 4483–4494, https://doi.org/10.1021/acs.jpcc.1c08914.
[30] Z. Wang, et al., Fluidity-Guided Assembly of Au@Pt on Liposomes as a Catalase-Powered Nanomotor for Effective Cell Uptake in Cancer Cells and Plant Leaves, ACS Nano (2022), https://doi.org/10.1021/acsnano.2c00327.
[31] J. Cardellini, C. Montis, F. Barbero, I. De Santis, L. Caselli, D. Berti, Interaction of Metallic Nanoparticles With Biomimetic Lipid Liquid Crystalline Cubic Interfaces, Front. Bioeng. Biotechnol. 10 (Mar. 2022), https://doi.org/10.3389/fbioe.2022.848687.
[32] L. Caselli, et al., A plasmon-based nanoruler to probe the mechanical properties of synthetic and biogenic nanosized lipid vesicles, Nanoscale Horiz. 6 (7) (2021) 543–550, https://doi.org/10.1039/D1NH00012H.
[33] D. Maiolo, et al., Colorimetric nanoplasmonic assay to determine purity and titrate extracellular vesicles, Anal. Chem. 87 (8) (2015) 4168–4176, https://doi.org/10.1021/ac504861d.
[34] A. Zendrini, et al., Augmented COlorimetric NANoplasmonic (CONAN) Method for Grading Purity and Determine Concentration of EV Microliter Volume Solutions, Front. Bioeng. Biotechnol. 7 (Feb. 2020), https://doi.org/10.3389/fbioe.2019.00452.
[35] J. Cardellini, et al., Probing the coverage of nanoparticles by biomimetic membranes through nanoplasmonics, J. Colloid Interface Sci. 640 (Jun. 2023) 100–109, https://doi.org/10.1016/j.jcis.2023.02.073.
[36] Y. Ma, et al., Near-infrared II phototherapy induces deep tissue immunogenic cell death and potentiates cancer immunotherapy, ACS Nano 13 (10) (2019) 11967–11980, https://doi.org/10.1021/acsnano.9b06040.
[37] A. Balestri, L. Chiappisi, C. Montis, S. Micciulla, B. Lonetti, D. Berti, Organized Hybrid Molecular Films from Natural Phospholipids and Synthetic Block Copolymers: A Physicochemical Investigation, Langmuir 36 (37) (2020) 10941–10951, https://doi.org/10.1021/acs.langmuir.0c01544.
[38] R.C. MacDonald, F.D. Jones, R. Qui, Fragmentation into small vesicles of dioleoylphosphatidylcholine bilayers during freezing and thawing, BBA - Biomembr. 1191 (2) (1994) 362–370, https://doi.org/10.1016/0005-2736(94)90187-2.
[39] F. Olson, C.A. Hunt, F.C. Szoka, W.J. Vail, D. Papahadjopoulos, Preparation of liposomes of defined size distribution by extrusion through polycarbonate membranes, BBA - Biomembr. 557 (1) (1979) 9–23, https://doi.org/10.1016/0005-2736(79)90085-3.
[40] S. Kim, K. Hyun, B. Struth, K.H. Ahn, C. Clasen, Structural Development of Nanoparticle Dispersion during Drying in Polymer Nanocomposite Films, Macromolecules 49 (23) (2016) 9068–9079, https://doi.org/10.1021/acs.macromol.6b01939.
[41] A. Ridolfi, et al., AFM-Based High-Throughput Nanomechanical Screening of Single Extracellular Vesicles, Anal. Chem. 92 (15) (2020) 10274–10282, https://doi.org/10.1021/acs.analchem.9b05716.
[42] D. Nečas, P. Klapetek, Gwyddion: an open-source software for SPM data analysis, Open Phys. 10 (1) (Jan. 2012), https://doi.org/10.2478/s11534-011-0096-2.
[43] Z.V. Leonenko, E. Finot, H. Ma, T.E.S. Dahms, D.T. Cramb, Investigation of temperature-induced phase transitions in DOPC and DPPC phospholipid bilayers using temperature-controlled scanning force microscopy, Biophys. J . 86 (6) (2004) 3783–3793.
[44] R. Seneviratne, R. Catania, M. Rappolt, L.J.C. Jeuken, P.A. Beales, Membrane mixing and dynamics in hybrid POPC/poly(1,2-butadiene- block -ethylene oxide) (PBd- b -PEO) lipid/block co-polymer giant vesicles, Soft Matter 18 (6) (2022) 1294–1301, https://doi.org/10.1039/D1SM01591E.
[45] M. Schulz, W.H. Binder, Mixed Hybrid Lipid/Polymer Vesicles as a Novel Membrane Platform, Macromol. Rapid Commun. 36 (23) (Dec. 2015) 2031–2041, https://doi.org/10.1002/marc.201500344.
[46] T.K. Lind, M. Cárdenas, H.P. Wacklin, Formation of supported lipid bilayers by vesicle fusion: Effect of deposition temperature, Langmuir 30 (25) (2014) 7259–7263, https://doi.org/10.1021/la500897x.
[47] G. Sauerbrey, Verwendung von Schwingquarzen zur Wägung dünner Schichten und zur Mikrowägung, Zeitschrift Für Phys. 155 (2) (1959) 206–222, https://doi.org/10.1007/BF01337937.
[48] B. Tenchov, R. Koynova, G. Rapp, New Ordered Metastable Phases between the Gel and Subgel Phases in Hydrated Phospholipids, Biophys. J . 80 (4) (Apr. 2001) 1873–1890, https://doi.org/10.1016/S0006-3495(01)76157-7.
[49] R. Richter, A. Mukhopadhyay, A. Brisson, Pathways of Lipid Vesicle Deposition on Solid Surfaces: A Combined QCM-D and AFM Study, Biophys. J . 85 (5) (2003) 3035–3047, https://doi.org/10.1016/S0006-3495(03)74722-5.
[50] I. Reviakine, D. Johannsmann, R.P. Richter, Hearing what you cannot see and visualizing what you hear: Interpreting quartz crystal microbalance data from solvated interfaces, Anal. Chem. 83 (23) (2011) 8838–8848, https://doi.org/10.1021/ac201778h.
[51] A. Ridolfi, et al., Gold nanoparticles interacting with synthetic lipid rafts: an AFM investigation, J. Microsc. 280 (3) (2020) 194–203, https://doi.org/10.1111/jmi.12910.
[52] X. Zhang, A. Lopez, Y. Liu, F. Wang, J. Liu, Interactions between citrate-capped gold nanoparticles and polymersomes, J. Phys. D Appl. Phys. 51 (24) (Jun. 2018), 244001, https://doi.org/10.1088/1361-6463/aac2b5.
[53] N.J. Lang, B. Liu, X. Zhang, J. Liu, Dissecting Colloidal Stabilization Factors in Crowded Polymer Solutions by Forming Self-Assembled Monolayers on Gold Nanoparticles, Langmuir 29 (20) (May 2013) 6018–6024, https://doi.org/10.1021/la3051093.
[54] X. Zhang, M.R. Servos, J. Liu, Ultrahigh Nanoparticle Stability against Salt, pH, and Solvent with Retained Surface Accessibility via Depletion Stabilization, J. Am. Chem. Soc. 134 (24) (Jun. 2012) 9910–9913, https://doi.org/10.1021/ja303787e.
[55] J. Teixeira, Small-angle scattering by fractal systems, J. Appl. Cryst. 21 (6) (1988) 781–785, https://doi.org/10.1107/S0021889888000263.
[56] B.A. Legg, M. Zhu, L.R. Comolli, B. Gilbert, J.F. Banfield, Impacts of Ionic Strength on Three-Dimensional Nanoparticle Aggregate Structure and Consequences for Environmental Transport and Deposition, Environ. Sci. Tech. 48 (23) (Dec. 2014) 13703–13710, https://doi.org/10.1021/es502654q.